# Sequence-dependent gating of an ion channel by DNA hairpin molecules

Veronica S. DeGuzman[1,2], Clarence C. Lee[3], David W. Deamer[4] and Wenonah A. Vercoutere[5,*]

[1]Ames Associate, Life Sciences Division, NASA Ames Research Center, Moffett Field, CA, USA, [2]MAP Pharmaceuticals, Palo Alto, CA, USA, [3]US Genomics, Woburn, MA, USA, [4]Center for Biomolecular Science and Engineering, University of California, Santa Cruz, CA 95064 and [5]Life Sciences Division, NASA Ames Research Center, Moffett Field, CA, USA

## ABSTRACT

**DNA hairpins produce ionic current signatures when captured by the alpha-hemolysin nano-scale pore under conditions of single molecule electrophoresis. Gating patterns produced by individual DNA hairpins when captured can be used to distinguish differences of a single base pair or even a single nucleotide [Vercoutere,W.A. *et al*. (2003) *Nucleic Acids Res.*, 31, 1311–1318]. Here we investigate the mechanism(s) that may account for the ionic current gating signatures. The ionic current resistance profile of conductance states produced by DNA hairpin molecules with 3–12 bp stems showed a plateau in resistance between 10 and 12 bp, suggesting that hairpins with 10–12 bp stems span the pore vestibule. DNA hairpins with 9–12 bp stems produced gating signatures with the same relative conductance states. Systematic comparison of the conductance state dwell times and apparent activation energies for a series of 9–10 bp DNA hairpins suggest that the 3′ and 5′ ends interact at or near the limiting aperture within the vestibule of the alpha-hemolysin pore. The model presented may be useful in predicting and interpreting DNA detection using nanopore detectors. In addition, this well-defined molecular system may prove useful for investigating models of ligand-gated channels in biological membranes.**

## INTRODUCTION

Scrutiny of short oligomers (<20 bp) has yielded rich detail about DNA structure and stability that has been valuable for understanding the biological functions of DNA [e.g. (1–5)]. In particular, investigating DNA hairpin molecules has helped elucidate the relationship between DNA hairpin dynamics and structure. These studies have helped clarify the function of hairpin and hairpin-like structures in biological activities where DNA zipping end dynamics are important, such as transcription, replication and repair (6–12). Methods including atomic force microscopy (13), optical tweezers (14) and molecular beacons (15) have recently been used to reveal the dynamics of DNA hairpin folding and unfolding at the single molecule level. A newly introduced method for examining single molecule DNA hairpins may be able to contribute to this area. In this method, unmodified nucleic acid is sampled from bulk phase using electrophoresis through a single nano-scale channel (16,17). A captured DNA or RNA molecule produces a characteristic ionic current blockade (18–25). The specific ionic current gating signatures may be used to discriminate among DNA hairpin molecules based on structural differences that correspond to differences in thermodynamic stability (16). Here we demonstrate the ability of the nanopore to discriminate among individual nucleotides at the terminus of DNA hairpin molecules, and propose a general model to relate the differences in molecular signatures detected by the pore to specific DNA conformational changes.

The nano-scale pore showing the highest sensitivity to individual DNA molecule structure and dynamics has been the alpha-hemolysin protein channel (16,17,26). The hemolysin pore self-assembles to form a heptameric structure with a 2.4 nm mouth defined by a ring of threonines, which leads into a wider vestibule (∼3.6 nm maximum diameter). The vestibule narrows to a 1.5 nm diameter limiting aperture defined by an alternating ring of lysines and glutamates, which is followed by a ∼2 nm diameter transmembrane stem (27) (Figure 1). The alpha-hemolysin pore has been used to study single-stranded (18,19,21,25,28,29) and double-stranded DNA (dsDNA) molecules (16,17,26,30–34). DNA is added to the *cis* side of the pore, and an applied potential

*To whom correspondence should be addresssed at NASA Ames Research Center, Mail Stop 236-7 Moffett Field, CA, USA. Tel: +1 650 604 6014; Fax: +1 650 604 3159; Email: wvercoutere@mail.arc.nasa.gov

The authors wish it to be known that, in their opinion, the first two authors should be regarded as joint First Authors
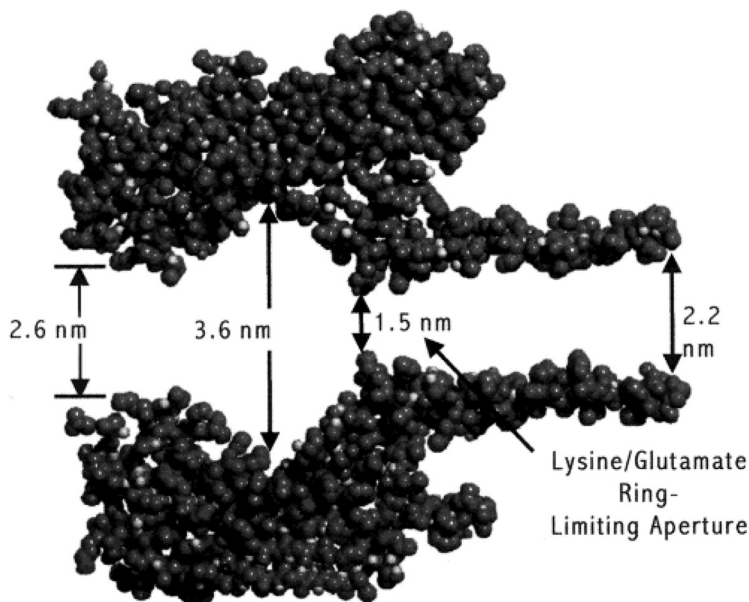
**Figure 1.** Cross section of the alpha-hemolysin ion channel showing the internal dimensions. The opening of the pore is 2.6 nm, which narrows slightly to 2.4 nm and then widens into the interior vestibule. The vestibule is 3.6 nm at its widest. The channel narrows again to the 1.5 nm limiting aperture, and ends with a 2.2 nm opening. [Image modified from Deamer and Branton (21)].
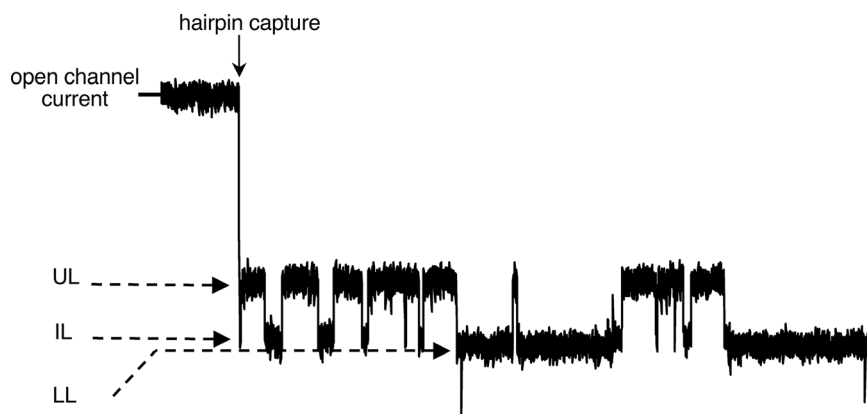


**Figure 2.** Ionic current signature produced by a single 9 bpC•G hairpin molecule captured in the alpha-hemolysin ion channel. Open channel current is shown (120 pA) terminating in a sharp drop in current that indicates the capture of the hairpin molecule. Ionic current is impeded by the captured hairpin in a characteristic blockade pattern that contains three conductance states with durations in the millisecond time scale. The conductance states are named according to the relative residual current (I/Io). Upper Level, UL, is ~48% I/Io, Intermediate Level, IL, is ~34% I/Io and Lower Level, LL is ~32% I/Io. A fourth conductance state level (S) spikes with very short life times to a near full blockade, ~14% I/Io. DNA hairpin molecules with stem lengths from 10 to 12 bp cause blockade signatures with the same relative conductance states, but with longer durations and less residual current for UL, IL and LL.

draws molecules one at a time into the vestibule and through the channel. Duplex DNA can enter the pore vestibule, while only single-stranded DNA (ssDNA) can translocate through the limiting aperture (16,31,34). Because of the relatively large dimensions of the alpha-hemolysin ion channel, water molecules in the pore can be regarded as bulk phase, except for at the narrow constriction at the limiting aperture (21,35,36). Models developed to describe DNA-pore interaction have been focused on single-stranded capture and translocation though the limiting aperture (37–42). Our studies are the first to present a model to explain how dsDNA captured in the alpha-hemolysin vestibule may modulate ionic current (17).

For DNA hairpins captured in the pore vestibule, the ionic current amplitude decreases in proportion to hairpin stem length. DNA hairpins with 3 through 7 bp stems produce a single amplitude blockade, or conductance state, from 68% residual current ($I/I_o$) caused by a 3 bp stem to 49% $I/I_o$ for a 7 bp stem. Blockade duration correlates directly with hairpin stability for hairpins with 3 to 8 bp stems (16).

Eight or nine base pair hairpins produce ionic current traces that transition between several discrete conductance states (16). The 9 bp hairpin gating signature has four conductance states (Figure 2). Changes in the terminal base pair identity alter the conductance level durations, but not amplitude. Three conductance states, at 49, 35 and 32%
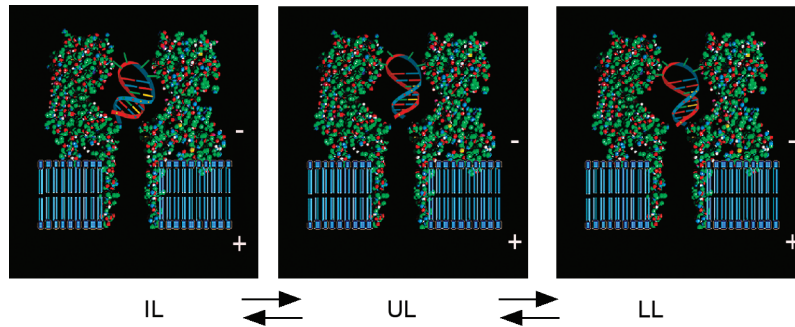
**Figure 3.** Proposed orientations of a DNA hairpin within the alpha-hemolysin vestibule, corresponding with conductance states IL, UL and LL (see conductance state transition pattern in Figure 2). The alpha-hemolysin channel is shown in cross section with a ribbon diagram figure of a DNA hp captured within the vestibule. Upon capture, the hairpin first produces the intermediate level conductance state (IL, left panel), and then transitions into upper level (UL, center panel). From UL, the ionic current blockade pattern produced by a DNA hairpin can transition to either IL or Lower Level (LL, right panel). Each panel corresponds with a conductance level, and depicts an orientation suggested by our results. The left panel shows the DNA hp terminus near the vestibule wall as suggested for IL; the center panel shows the DNA base pair stem oriented along the central axis, as proposed for UL; the right panel shows the DNA terminus shifted just off the central axis to indicate association at or near the limiting aperture, as proposed for LL. [Image modified from (21)]

$I/I_o$, have dwell times in the millisecond range. These low-frequency states were designated as upper level (UL), intermediate level (IL) and lower level (LL), based on the relative current amplitude measured for each state (16,17). The fourth conductance state corresponds to high-frequency current deflections from the LL to near full blockade, which we designated the spike level (SL). The spike events result from the DNA duplex fraying at its terminus and one frayed strand extending toward the limiting aperture; this is the subject of a separate study (DeGuzman,V.S. manuscript in preparation). DNA hairpins remain base paired while producing the characteristic ionic current blockades, because mismatches placed higher in hp sequence that destabilize the hairpin shorten the duration, but do not alter the amplitude or pattern of the gating event, [(16) for 6 bp hairpin; data not shown for 9 bp hairpins]. This also suggests that the strength of the potential field on the hairpin terminus is equal to or less than the ∼12–14 pN required to rapidly unzip duplex DNA (13,31,43). Watson–Crick base pair identity and orientation at the terminus of individual 9 bp hairpin molecules can be distinguished (17,26). The differences in gating patterns correspond to differences in $\Delta G$, free energy of formation (17). To elucidate DNA sequence-dependent end dynamics using this detector, it is critical to have an understanding of the physical conformational changes or DNA–protein interactions that account for the differences in gating patterns.

Previously, we proposed a mechanistic model where the low-frequency conductance states are due to the orientation of the DNA hairpin within the alpha-hemolysin vestibule, and may include transient association of the terminal base pair with the vestibule interior (Figure 3) (17). In our model, the blunt end of the hp is drawn into the vestibule, while the hairpin loop is unable to enter (16). Using the crystal structure of the hemolysin channel (27), we calculate that the 33 Å distance between threonines (T9) at the vestibule mouth and the lysines (K147) forming the limiting aperture is approximately equivalent to the length of a 10 bp DNA duplex (3.4 Å/bp). We therefore predict that hairpins at 10 bp or longer may reach the limiting aperture. Detection of differences may be most sensitive to the terminus of DNA hairpins ∼10 bp long because of the proximity to the strongest part of the potential field. Upon capture of a 9 bp DNA hairpin molecule, our model proposes that the initial state, the IL (see Figure 2), is due to an electrostatic interaction between the terminal base pair and residues in the vestibule wall. We predicted that the dwell time for this intermediate conductance state is largely independent of base pair identity or orientation, presumably because the interaction with the protein surface is electrostatic. The IL state invariably transitions to the upper conductance state, UL. In our model, this state corresponds to desorption of the terminal base pair from the protein wall and thermal motion of the hairpin stem in central or angular orientations that allow greater ion current flow through the limiting aperture. From the UL conductance state, the hairpin may return to the IL state or it may transition into a third conductance state, LL. Residence time in the LL is dependent on terminal base pair identity and orientation. We hypothesize that the LL is produced when one or both terminal nucleotides of the duplex stem adsorbs to the protein in close proximity to the pore-limiting aperture. In this orientation, the terminal base pair interacts significantly with the ion current at the limiting aperture.

The aim of this work is to test the proposed model. We examined a series of DNA hairpin molecules with stem lengths ranging from 3 to 12 bp using the alpha-hemolysin pore detector, and applied kinetic analysis to the current gating signatures. DNA hairpins with 9–12 bp produced gating signatures with the same relative conductance states, IL, UL, LL and SL. To probe the sensitivity of the nanopore detector to changes in DNA and to investigate the underlying mechanism, we measured conductance state dwell times and activation energy of transitions among the IL, UL and LL conductance states. We examined ionic current blockades produced by 9 bp hairpins with either: (i) a 5′ phosphate, abasic or nucleotide overhang, (ii) a 3′ phosphate, abasic or nucleotide overhang, and 10 bp hairpins with either (iii) a Watson–Crick terminal base pair or (iv) a terminal base pair mismatch. Nucleotide identity and orientation affected

**Table 1.** Sequences of DNA hairpins used for stem resistance analysis (Figure 3)

| Predicted hairpin secondary structure | | | | | | | | | | |
|---|---|---|---|---|---|---|---|---|---|
| TT | TT | TT | TT | TT | TT | TT | TT | TT | TT |
| T  T | T  T | T  T | T  T | T  T | T  T | T  T | T  T | T  T | T  T |
| G C | G C | G C | G C | G C | G C | G C | G C | G C | G C |
| C G | C G | C G | C G | C G | C G | C G | C G | C G | C G |
| C G | A T | A T | A T | A T | A T | A T | A T | A T | A T |
|  | C G | A T | A T | A T | A T | A T | A T | A T | A T |
|  |  | C G | G C | G C | G C | G C | G C | G C | G C |
|  |  |  | C G | T A | C G | C G | C G | C G | C G |
|  |  |  |  | C G | T A | T A | T A | T A | T A |
|  |  |  |  |  | C G | T A | T A | T A | T A |
|  |  |  |  |  |  | C G | C G | C G | C G |
|  |  |  |  |  |  |  | C G | G C | A A |
|  |  |  |  |  |  |  |  | C G | T A |
|  |  |  |  |  |  |  |  |  | C G |
| **Stem length (bp)** | | | | | | | | | |
| 3 | 4 | 5 | 6 | 7 | 8 | 9 | 10 | 11 | 12 |
| **$\Delta G^{\circ}_{23}$ (kcal/mol)** | | | | | | | | | |
| −3.0 | −4.4 | −5.7 | −8.1 | −8.9 | −11.3 | −12.6 | −14.7 | −17.7 | −14.7 |

The free energy of formation ($\Delta G^{\circ}_{23}$) for each hairpin was calculated using Mfold (45).

dwell times and activation energies of transition among the IL, UL and LL conductance states. We found that the 3′ and 5′ ends individually produce different types of changes to the ionic current gating signatures, indicating that a different type of interaction occurs between each end and the protein channel field. Our results support and expand on our model describing how single DNA molecules modulate ionic current when captured in an alpha-hemolysin pore, and show how this tool may be used to examine the end dynamics of single molecule DNA. The improved model is intended to provide further context for predicting and interpreting DNA detection using nanopore detectors. Because the ion channel and DNA structures are known, this system may also prove useful as a model of ligand-gated ion channels.

## MATERIALS AND METHODS

### Materials

Nucleotides used for the synthesis of DNA duplexes were purchased from Glen Research (Sterling, VA). The membrane pore protein, alpha-hemolysin, was purchased from Calbiochem (San Diego, CA). Diphytanoyl-phosphatidylcholine was obtained from Avanti Polar Lipids (Alabaster, AL) and was used without further purification. All other chemicals were purchased from Fisher Scientific unless otherwise noted.

### DNA hairpin synthesis

DNA oligonucleotides were synthesized using an ABI 392 synthesizer (Foster City, CA). The DNA oligonucleotides were purified by PAGE and stored at −70°C in TE buffer. In the series of DNA hairpin molecules containing 3–12 bp, the sequence of the DNA hairpin stems were varied by either adding or removing base pairs from a well characterized 6 bp hairpin (44). The prediction that each hairpin would adopt one base paired structure at 23°C was confirmed using the DNA Mfold web server (45). For the series of DNA hairpin molecules containing between 9 and 10 bp, a single phosphate, abasic or nucleotide overhang was added on either the 5′ or 3′ end or to both ends on a core 9 bp hairpin sequence (Table 1). All hairpin loops were composed of 4dT and were closed with a G•C base pair. The DNA Mfold web server was used to calculate the base paired structure and $\Delta G$ for each hairpin at 23°C (45).

### Hemolysin pore in a lipid bilayer

Each experiment was done with a single alpha-hemolysin channel inserted into a diphytanoyl-phosphatidylcholine/ hexadecane bilayer as described in previous reports. Briefly, the bilayer is formed across a 20 μm diameter horizontal Teflon aperture (18). Two 70 μl chambers are separated by the bilayer, each containing KCl buffer [1 M KCl and 10 mM HEPES (pH 8.0)]. Voltage is applied across the bilayer using Ag-AgCl electrodes. The elimination of ionic current indicates the successful formation of a bilayer between the chambers. With the bilayer in place, a dilute solution of monomeric alpha-hemolysin is added to the *cis* chamber. Self-assembly of the protein subunits into a stable heptameric pore inserted across the bilayer results in a steady current under an applied voltage. Once a channel inserts into the bilayer, the excess monomer subunits are perfused from the *cis* chamber to prevent the formation of more protein pores in the bilayer.

### Data acquisition

To investigate a given DNA molecule, the oligonucleotide was added to the *cis* chamber to a final concentration of 10 μM. Experiments were run at temperatures ranging from 10 to 44°C, with the temperature controlled by a Newport 350 temperature controller (Irvine, CA) combined with a customized Peltier device. An experiment is defined as the set of ionic current data for a particular molecule collected from one channel. Ionic current was monitored at 50 kHz bandwidth using a lowpass (10 kHz) Bessel filter and recorded at 20 μs intervals (50 kHz), using an Axopatch 200B amplifier (Axon Instruments, Foster City, CA) coupled to an Axon Digidata 1320A digitizer. An applied potential of 120 mV with *trans* side positive was used for all experiments, which produced an open channel current ($I_o$) of 120 ± 5 pA with 1.0 M KCl at 23°C.

### Data analysis

Analysis of current blockade amplitudes and durations was performed using Fetchan 6.0, 6.01 and Clampfit 9.0, 9.2 (Axon Instruments) on data filtered at 2 kHz using a digital lowpass Gaussian filter (Axon Instruments). In unusual cases (<10% of signals), the current blockades and amplitude differences between conductance states for a single hairpin type were markedly different from typical signals, and these data points were not included in the analysis.

Resistance (R) was calculated using $V = IR$, where $V =$ applied potential and $I =$ experimentally determined residual current of a given conductance state. Conductance state dwell times (tau, $\tau$) were determined as an ensemble average of the single molecule event data using Clampfit 9.0, 9.2 (Axon Instruments). Scatter plots of amplitude versus duration were used to verify a single population. For each conductance state, $\tau$ was determined using a log plot of conductance state event durations. Dwell time histograms were best fit using a single-term log probability function. Intermediate level tau, $\tau_{IL}$, refers to the weighted mean duration of IL before a transition to UL. LL tau, $\tau_{IL}$, refers to the weighted mean duration of LL before a transition to UL. UL tau, $\tau_{UL}$, refers to the weighted mean duration of UL before a transition to IL or LL. The tau values for UL transitions to IL or to LL were not significantly difference, and therefore were calculated as one value.

To calculate activation energy ($E_a$) for each conductance state, dwell rate was obtained as the inverse of dwell time (46). The value of $E_a$ is the product of the slope from an Arrhenius plot, ln(dwell rate) against 1/T (in Kelvin), and the ideal gas constant ($-8.314$ J/K). For the purposes of

analysis, the number of hairpin exit transitions (translocation) was <1% compared to transitions from IL to UL or LL to UL. Thus IL $E_a$ refers to the activation energy required to transition from IL to UL, and LL $E_a$ refers to the energy required to transition from LL to UL. The UL $E$a gives the energy required to transition from UL to either IL or LL.

## RESULTS

### Conductance state resistance reached a plateau as hairpin stem lengthened to 12 bp

We measured conductance state amplitude and duration for DNA hairpin molecules with 3–12 bp stems, and calculated resistances in Gohm (Figure 4). Within a gating event, the number of conductance states and the amplitude of conductance states depended on stem length. As shown previously, DNA hairpins with 3–7 bp stems each produced a single conductance state, and the 8 bp hairpin produced ionic current gating events that transitioned between two conductance states, with resistances of 35 and 49% $I/I_o$ (16). Resistance values increased incrementally from 0.5 to 1 Gohm.

With these experiments, we observed for the first time that hairpins with 9 bp through 12 bp stems produced ionic current blockades that transitioned among three millisecond time scale conductance states. DNA hairpins with more than 12 bp produced a near full, long-duration blockade that did not show a gating pattern. For example, a 21 bp DNA hairpin caused a single conductance state blockade with a resistance of 2.85 Gohm (see Figure 4). For each
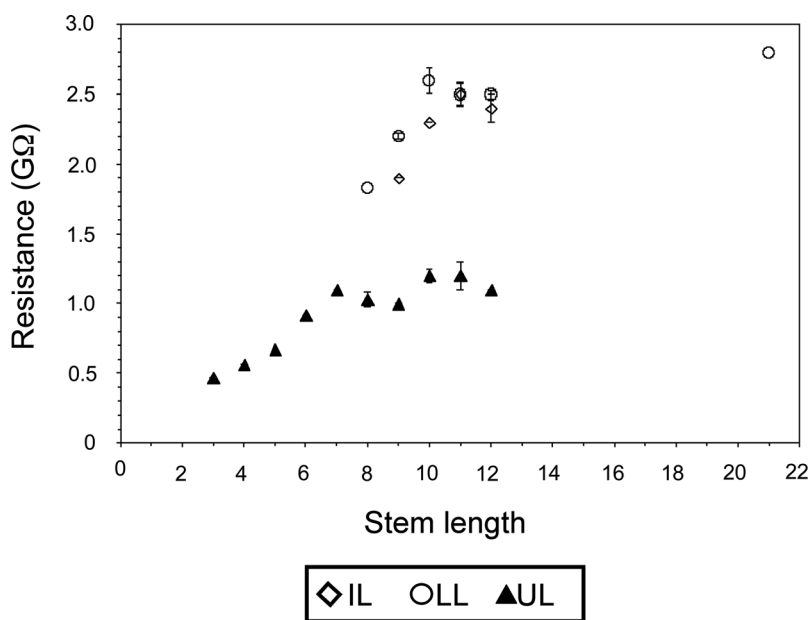


**Figure 4.** Ionic current resistance produced by hairpins with increasing stem lengths. 3–7 bp hairpins show a single conductance level, which we interpreted as corresponding to upper level, UL (solid triangles). Hairpin molecules with 8 or more base pairs showed additional conductance states: intermediate level, IL (open diamonds), and lower level, LL (open circles). IL and LL resistance values overlapped for 11 and 12 bp hairpins. Resistance curves for IL and LL conductance levels plateau at 2.5 Gohms, for UL at 1.3 Gohms. DNA hairpins with more than 12 bp produced a near full, long-duration blockade that did not show a gating pattern. The example shown was a 21 bp DNA hairpin, which caused a single conductance state blockade (which we interpret as LL) with a resistance of 2.85 Gohm. Each value was calculated from at least three experiments. Error bars represent standard error; for some data, the symbol is larger than the span of the error bar.

DNA hairpin length, the conductance states had the same relative amplitude levels corresponding to the IL, UL and LL identified previously for the 9 bp hairpin (17). For each additional base pair from 9 to 12 bp, all three conductance states showed deeper amplitudes and longer durations. A plot of resistance values for all conductance states as a function of hairpin stem length (number of base pairs) shows the resistance values for the single conductance state events (i.e. 3–7 bp hp events) were close in value to the resistance calculated for the UL of the two- and three-level events. The data for the other two conductance levels, IL and LL, overlap (Figure 4). Overall, the plotted data reach a plateau at two resistance values. Our model can explain this division in resistance values. Our model asserts that a captured hairpin is in a bound or unbound orientation, where the unbound state has a lower resistance than the bound state. The unbound state is equivalent to the UL in the 8–12 bp hairpin gating events. Hairpins with stems less than 8 bp are too short to reach a bound orientation and only exhibit the unbound resistance value. Therefore, the 3–7 bp resistance values correspond to the UL conductance state; we have labeled them accordingly. As suggested by the physical dimensions of the pore depth and dsDNA length, the resistance curve plateau provides further indication that hairpins with 9–12 bp span the pore vestibule from mouth to limiting aperture.

## Conductance state dwell times depend on identity of terminal nucleotide(s)

Our results here showed that hairpins with 9 to 12 bp stems produced the same relative conductance states. We therefore hypothesize that the same mechanism may explain the gating patterns produced 9–12 bp DNA hairpins. Our model predicts that the millisecond time scale conductance states produced by 9–12 bp DNA hairpins captured in the alpha-hemolysin pore correspond to different bound or unbound orientations of the hp stem within the pore vestibule, and that the stability of the bound or unbound orientations is dependent upon the identity of the terminal nucleotide(s). The stability of these orientations may also correlate with the change in free energy of formation ($\delta\delta G$) for each molecule (Table 2). To test the predictions of our model, we made changes to the 5′ and/or 3′ ends of a core 9 bp hairpin sequence and measured the effects on the dwell time, $\tau$, for each conductance state. For a subset of the molecules tested, we also measured the temperature dependence of the gating patterns and calculated apparent activation energy. The DNA hairpins we examined consisted of a 22mer, 9 bp C•G, as the core structure with an additional nucleotide (10 bpN•- or 10 bp-•N) or pair of nucleotides (10 bpN•N) added to the terminus. To test the contribution to the blockade duration from charge and shape, we examined the 9 bpC•G with a phosphate or an abasic overhang on the 5′ side [9 bp Cp•G or 9 bp (C/ab)•G] or the 3′ side [9 bp C•Gp or 9 bp C•(G/ab)]. Phosphorylation of either the 5′ or the 3′ end tested the effects of additional negative charge without significant additional length. An abasic phosphate-sugar backbone overhang on either the 5′ or 3′ end tested the effects of additional charge and length. The abasic overhang also offered a negative control for possible steric and hydrogen bond interactions involving the nucleotide base. We used a 10 bpT•T hairpin to investigate

**Table 2.** $\delta\delta G$ for hairpin molecules using $\Delta G^{\circ}_{23}$ for the core 9 bpCG sequence as the reference. These values were generated from the Mfold free energy of formation ($\Delta G^{\circ}_{23}$) for each hairpin (45)

| | $\delta\delta G$ from 9 bpC•G 10 bpN•- | 10 bp-•N |
|---|---|---|
| (A) With a single nucleotide overhang | | |
| Terminal nucleotide | | |
| C | −0.70 | −0.23 |
| T | −0.73 | −0.53 |
| G | −0.92 | −0.60 |
| A | −1.20 | −0.97 |
| (B) With a blunt end | | |
| Terminal base pair | | |
| T—T | −1.26 | |
| T•A | −1.46 | |
| T—A | −1.70 | |
| A•T | −1.60 | |
| A—T | −1.73 | |
| C•G | −2.12 | |
| G•C | −2.58 | |

the affect on dwell time of the presence of nucleotides on both side with reduced base pair hydrogen bonding.

We expect 5′ and 3′ ends to produce a difference even with the same charge or nucleotide because of configuration differences. We also expect different charge or nucleotides at the same end to have different interactions. However, these differences depend on what is presented to the protein—i.e. ribose or phosphate, compared to a complete nucleotide. We reasoned that if no difference is measured, then interactions, if any, do not involve that which was changed. If the terminus of the DNA does not interact with the pore, then variations in the terminus would cause little to no difference in the conductance state durations, or a random difference to conductance state durations. If, however, a change at the terminus produces a difference in one or more conductance state durations, then interaction between the DNA and the pore is implied.

Kinetic analysis of the ionic current gating patterns showed that the dwell time pattern for each DNA hairpin molecule examined was unique and distinguishable from the others (Tables 3 and 4). Overall, the dwell times for UL, IL and LL for the 10 bp hairpins with Watson–Crick base pairing along the stem were nearly all greater than values obtained for the 9 bpC•G and corresponding overhang hairpins (10 bpN•- or 10 bp-•N). For each conductance state, trends in the affect from altering the terminal position were discernable. Among the three conductance states UL, IL and LL, dwell time changes differed in magnitude, with increases in duration for IL and UL ranging between 1 and 26×, and increases in LL durations ranging from 20 to 60×.

*Intermediate level dwell times.* Our model predicts that IL dwell times are due to an electrostatic interaction between the terminal base pair and residues within the vestibule wall, and are independent of base pair identity or orientation. We found that the 5′ overhangs (including phosphorylated and abasic) resulted in little or no change in IL duration. $\tau_{IL}$ values ranged from 1 to 7 ms (Table 3). $\tau_{IL}$ increased more with the addition of an overhang in the 3′ position (including phosphorylated and abasic) (Table 3). Compared to the 2 ms $\tau_{IL}$ for 9 bpC•G, the 9 bpC•Gp showed an increase in $\tau_{IL}$ to 22 ms, and the 9 bpC•(G/ab) increased

**Table 3.** Conductance state dwell times for DNA hairpins with overhangs

| Terminal nucleotide | Dwell time in ms at 23°C ± SE | |
| --- | --- | --- |
| | 10 bpN•- | 10 bp-•N |
| IL | | |
| Phosphate | 2 ± 0.01 | 22 ± 0.10 |
| Abasic | 1 ± 0.02 | 11 ± 0.01 |
| A | 7 ± 0.01 | 42 ± 0.10 |
| G | 6 ± 0.03 | 38 ± 0.06 |
| T | 3 ± 0.01 | 46 ± 0.14 |
| C | 4 ± 0.02 | 30 ± 0.05 |
| UL | | |
| Phosphate | 7 ± 0.01 | 20 ± 0.10 |
| Abasic | 20 ± 0.02 | 47 ± 0.03 |
| A | 7 ± 0.02 | 22 ± 0.05 |
| G | 21 ± 0.06 | 51 ± 0.09 |
| T | 16 ± 0.24 | 73 ± 0.16 |
| C | 11 ± 0.01 | 29 ± 0.05 |
| LL | | |
| Phosphate | 47 ± 0.21 | 166 ± 2.0 |
| Abasic | 242 ± 9.0 | 39 ± 0.03 |
| A | 206 ± 1.20 | 40 ± 0.16 |
| G | 241 ± 1.83 | 53 ± 0.21 |
| T | 93 ± 0.19 | 40 ± 0.13 |
| C | 127 ± 0.10 | 49 ± 0.20 |

Errors represent SE at 99% confidence level. Each value was calculated from at least three experiments, where each experiment contained ∼3000 conductance events.

**Table 4.** Conductance state dwell times for blunt-ended DNA hairpins

| Terminal base pair | Dwell time in ms at 23°C ± SE |
| --- | --- |
| IL | |
| T--T | 30 ± 0.12 |
| TA | 40 ± 0.12 |
| AT | 79 ± 0.25 |
| CG | 49 ± 0.32 |
| GC | 56 ± 3.08 |
| UL | |
| T--T | 49 ± 0.24 |
| TA | 23 ± 0.07 |
| AT | 212 ± 0.83 |
| CG | 140 ± 1.31 |
| GC | 101 ± 10.3 |
| LL | |
| T--T | 155 ± 1.31 |
| TA | 627 ± 4.67 |
| AT | 1653 ± 26.6 |
| CG | 2778 ± 92.2 |
| GC | 8013 ± 149 |

Errors represent SE at 99% confidence level. Each value was calculated from at least three experiments, where each experiment contained ∼3000 conductance events.

$\tau_{IL}$ to 11 ms. $\tau_{IL}$ for hairpins with 3′ nucleotides ranged from 30 to 46 ms. Paired bases at the terminus increased $\tau_{IL}$ greater than the sum of the corresponding individual 5′ and 3′ overhangs, except for the 10 bpT•A (Table 4). The presence of a purine in the 5′ position produced longer $\tau_{IL}$ relative to base pair with the purine in the 3′ position. The 10 bpT•T hairpin $\tau_{IL}$ was shorter (30 ms) than the $\tau_{IL}$ for 10 bp-•T (46 ms). The $\tau_{IL}$ for each blunt-ended molecule was in some cases less than and in some cases greater than the sum of $\tau_{IL}$ for hairpins with 5′ and 3′ overhangs corresponding to the blunt-ended molecule. Although the increases in $\tau_{IL}$ for hairpins with 5′ overhangs were small, they corresponded with the increase in $\delta\delta G$ of the molecules. The $\tau_{IL}$ increases for hairpins with 3′ overhangs did not correlate with $\delta\delta G$ of the molecules. Changes in $\tau_{IL}$ for blunt-ended molecules also did not correlate with $\delta\delta G$ of the molecules. Consistent with our model, these results indicate a role for the 3′ end phosphate-sugar backbone in IL conductance state, but also suggest a role for the nucleotide base identity.

*Upper level dwell times.* Our model hypothesizes that UL corresponds to an orientation of the hairpin with the terminal base pairs desorbed from the vestibule interior. This would allow the hairpin to interact more freely with the potential field. If correct, our model predicts increased dwell time to result from increased charge on the hairpin end. Because UL transitions to both IL and LL, we also might expect two different lifetimes for UL. However, no significant difference resulted for these two transitions. A single dwell time value corresponding to transition to either IL or LL was therefore calculated for UL. Compared to the 8 ms $\tau_{UL}$ for 9 bpC•G, DNA hairpins with 5′ overhangs (including phosphorylated and abasic) showed little or no change in UL duration; $\tau_{UL}$ values ranged from 7 to 21 ms (Table 3). All tested 3′ overhangs (including phosphorylated and abasic) increased UL dwell times. 3′ Phosphorylation increased $\tau_{UL}$ to 20 ms, and 3′ abasic increased $\tau_{UL}$ to 47 ms. 3′ Single nucleotide overhangs increased $\tau_{UL}$ ranging from 22 to 73 ms. The presence of a Watson–Crick terminal base pair increased $\tau_{UL}$ by 2.5 times for 10 bpT•A, and increased the change in duration more—between 12 and 26 times—for the other three terminal base pairs (A•T, C•G and G•C) (Table 4). There was no pattern for dependence on orientation, identity or number of hydrogen bonds. The mismatch on the 10 bpT•T hairpin also increased $\tau_{UL}$, to 49 ms. The $\tau_{UL}$ for each blunt-ended molecule did not equal the sum of $\tau_{UL}$ for hairpins with 5′ and 3′ overhangs corresponding to the blunt-ended molecule. $\tau_{UL}$ increases for hairpins with 5′ or 3′ overhangs did not correlate with $\delta\delta G$ of the molecules. Changes in $\tau_{UL}$ for blunt-ended molecules also did not correlate with $\delta\delta G$ of the molecules. We conclude that the 3′ end has a greater impact on UL conductance state dwell time.

*Lower level dwell times.* Our model predicts that in the LL conductance state one or both hairpin terminal ends directly interact with residues at or near the limiting aperture. Consistent with our model, modifications to either terminus affected lower level dwell time ($\tau_{LL}$). 5′ Overhangs increased $\tau_{LL}$, with the exception of a 5′ phosphate, which did not change $\tau_{LL}$ (47 ms) (Table 3). 3′ Overhangs decreased $\tau_{LL}$, in the range of 34–53 ms, compared to $\tau_{LL}$ for 9 bpC•G (52 ms). The exception was a 3′ phosphate, which increased $\tau_{LL}$ (166 ms). The biggest effect to $\tau_{LL}$ resulted from the presence of a Watson–Crick base pair at the terminus. Both the identity and orientation of the terminal base pair affected $\tau_{LL}$ (Table 4). The order of increasing $\tau_{LL}$ for the terminal base pairs was: T•A < A•T < C•G < G•C. Specifically, the 10 bpT•A $\tau_{LL}$ was 12× longer than the 9 bpC•G, 10 bpA•T $\tau_{LL}$ was 33× longer, the 10 bpC•G was 54.5× longer, and the 10 bpG•C was 160× longer. The dwell time for the 10 bpT•T mismatch, 155 ms, was also greater than for either 5′ or 3′ overhang alone. The $\tau_{LL}$ for each blunt-ended molecule was greater than the sum of $\tau_{LL}$ for hairpins

with 5′ and 3′ overhangs corresponding to the blunt-ended molecule. The $\tau_{LL}$ increases for hairpins with 5′ or 3′ overhangs did not correlate with $\delta\delta G$ of the molecules. However, changes in $\tau_{LL}$ for blunt-ended molecules correlated with $\delta\delta G$ of the molecules. These results support the premise that the LL conductance state is a result of interactions between the protein and both terminal ends.

### Terminal nucleotide identity and 5′ versus 3′ orientation affect conductance state stability

We next determined the apparent activation energies ($E_a$) required for transitions among the 10 bp ionic current gating conductance states using a subset of the molecules examined for changes in conductance state duration. We measured the affect of temperature on conductance state durations ($\tau$) for 9 bp hairpins with an abasic overhang on the 5′ side or the 3′ side, and for DNA hairpins with single nucleotide overhangs, 10 bpT•-, 10 bpA•-, 10 bp-•T and 10 bp-•A, and 10 bpT•A, 10 bpA•T and the mismatch 10 bpT•T. We reasoned that the magnitude of differences in activation energies among conductance states for molecules in this set would indicate the type of interaction or interactions that were taking place. This could include steric, hydrogen bonding or electrostatic interactions with the protein, or configuration shifts in the DNA. We found that orientation and identity of the nucleotide(s) at the terminal end affected activation energies for transitions among conductance states (Table 5). Compared with the blunt-ended DNA hairpins, both 5′ and 3′ overhang molecules had lower activation energies for all three conductance levels. The presence of a 5′ overhang lowered the apparent activation energy for IL and UL more than a 3′ overhang, while the LL activation energy

was lowered more by the presence of a 3′ overhang than a 5′ overhang (Figure 5A–C).

*Intermediate level activation energy.* Activation energy for IL transitions did not change for the 9 bp(C/ab)•G, and modestly increased for the 9 bpC•(G/ab), compared to 9 bpC•G (Table 5). The 5′ A or 5′ T overhang stabilized IL by 3 or 5 kcal/mol relative to the 9 bpC•G. The IL activation energy values for DNA molecules with a 3′ nucleotide in the terminal position, 10 bp-•A and 10 bp-•T, were comparable to hairpins with Watson–Crick base pairs at the terminus, 10 bpA•T (solid line, Figure 5A) and 10 bpT•A (solid line, Figure 5B). The largest change in activation energy was for 10 bpT•A and 10 bp-•A, where $E_a$ for each molecule increased by ~10 kcal/mol. Similarly, 10 bpA•T, 10 bpT•T mismatch (solid line, Figure 5C), and 10 bp-•T each showed ~9 kcal/mol increase in $E_a$ relative to the 9 bpC•G. These differences in activation energy suggest that the terminal 3′ end governs the IL conductance state while the 5′ end has minimal influence.

*Upper level activation energy.* Activation energy for UL transitions increased by 2 kcal/mol for 9 bp(C/ab)•G, and by 10 kcal/mol for 9 bpC•(G/ab), compared to 9 bpC•G (Table 5). The UL activation energies for the 5′ overhang molecules 10 bpT•- and 10 bpA•- were unchanged compared to 9 bpC•G, while the UL activation energies for the 3′ overhang molecules 10 bp-•A and 10 bp-•T were greater by 5 or 7 kcal/mol. The UL activation energies for 10 bpA•T (solid line, Figure 5A), 10 bpT•A (solid line, Figure 5B) and 10 bpT•T (solid line, Figure 5C) were greater than for the DNA hairpins with 5′ or 3′ overhangs. The largest change in UL activation energy was for 10 bpA•T, where $E_a$ increased by 16 kcal/mol. The activation energies for 10 bpT•A and 10 bpT•T increased by about 13 kcal/mol compared to the 9 bpC•G. This suggests that the 3′ terminal end is also a determining factor for the UL conductance state $E_a$.

*Lower level activation energy.* Activation energy for LL transitions increased 4 kcal/mol for 9 bp(C/ab)•G and 3 kcal/mol for 9 bpC•(G/ab), compared to 9 bpC•G (Table 5). The LL activation energies for the 5′ and the 3′ overhang molecules were similar. The LL activation energy for 10 bpT•- and 10 bpA•- increased by 8 or 5 kcal/mol, and 10 bp-•A increased by 8 kcal/mol compared to 9 bpC•G. The only reduction in LL activation energy was for 10 bp-•T, which decreased by about 1 kcal/mol. The LL activation energies for 10 bpA•T (solid line, Figure 5A), 10 bpT•A (solid line, Figure 5B) and 10 bpT•T (solid line, Figure 5C) were greater than for the DNA hairpins with 5′ or 3′ overhangs. The largest change in LL activation energy was for 10 bpT•A, where $E_a$ increased by about 28 kcal/mol. Other than the 10 bp-•T, activation energies for LL transitions increased for all molecules. This indicates a combined effect on the lower level activation energy from both the 5′ and 3′ position.

**Table 5.** Apparent activation energies in kcal/mol for 9–10 bp hairpins

| Terminal nucleotide | Ea (kcal/mol) | |
| --- | --- | --- |
| | 10 bpN•- | 10 bp-•N |
| IL → UL | | |
|   9 bpC•G | | 18 ± 1.0 |
|   Abasic | 18.0 ± 1.0 | 21.0 ± 2.0 |
|   T | 23.2 ± 0.5 | 26.3 ± 1.4 |
|   A | 20.9 ± 1.2 | 28.3 ± 1.2 |
|   T--T | 27.5 ± 1.4 | |
|   TA | 28.4 ± 0.7 | |
|   AT | 25.9 ± 1.7 | |
| IL ← UL→ LL | | |
|   9 bpC•G | | 13 ± 1.0 |
|   Abasic | 15.0 ± 1.0 | 23.0 ± 2.0 |
|   T | 14.5 ± 0.9 | 21.5 ± 0.8 |
|   A | 13.3 ± 2.9 | 17.5 ± 1.9 |
|   T--T | 24.0 ± 1.5 | |
|   TA | 25.7 ± 1.2 | |
|   AT | 29.0 ± 2.0 | |
| LL → UL | | |
|   9 bpC•G | | 15 ± 1.0 |
|   Abasic | 19.0 ± 1.0 | 18.0 ± 1.0 |
|   T | 22.6 ± 2.0 | 13.3 ± 1.4 |
|   A | 20.4 ± 2.5 | 22.7 ± 1.8 |
|   T--T | 30.7 ± 1.3 | |
|   TA | 43.7 ± 1.4 | |
|   AT | 36.6 ± 2.8 | |

Errors represent SE at 99% confidence level. Each value was calculated from at least three experiments, where each experiment contained ~3000 conductance events.

## DISCUSSION

In this study, we tested our proposed model describing the molecular mechanism underlying how individual DNA hairpin molecules cause unique ionic current gating
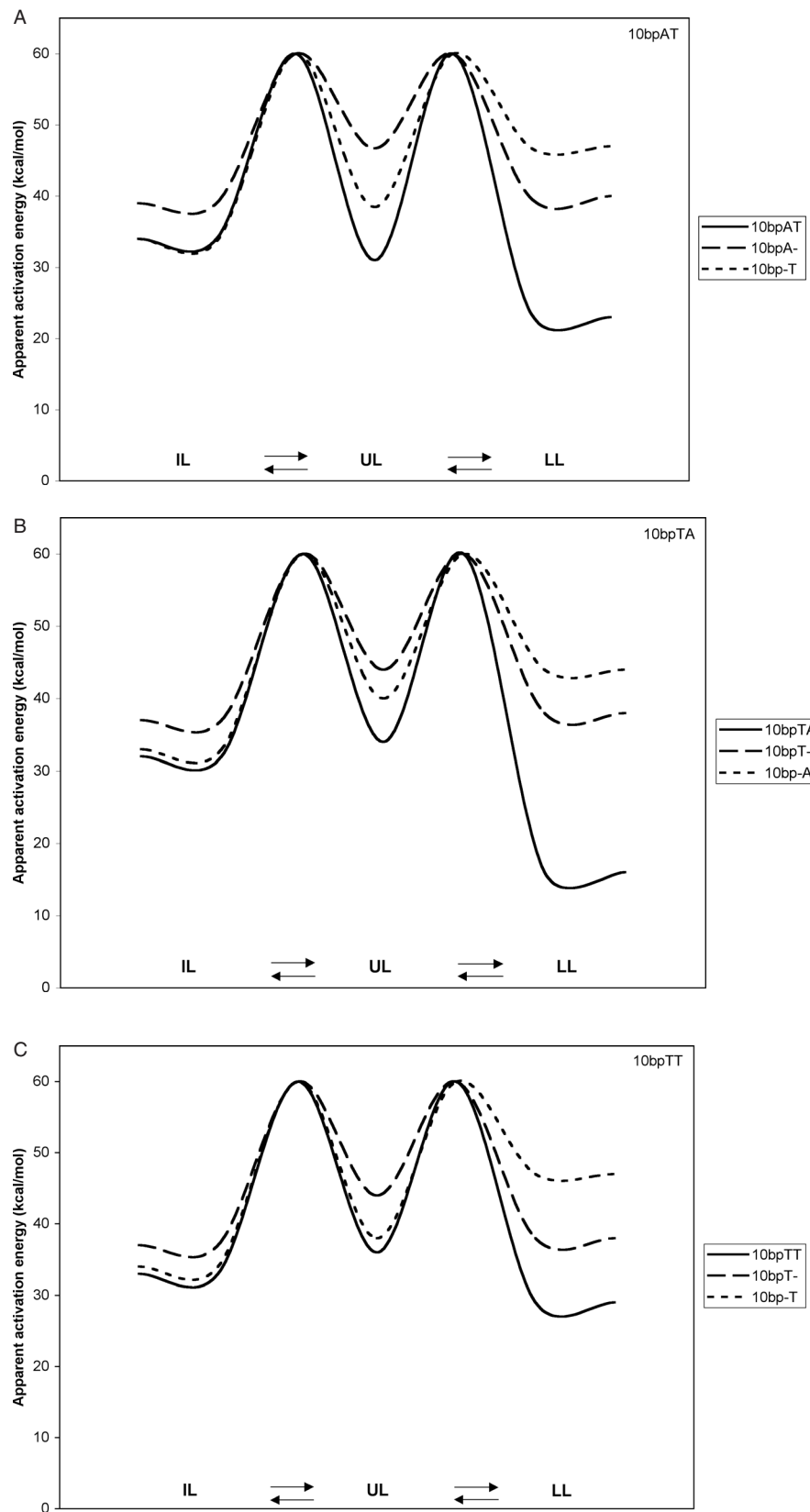
**Figure 5.** Reaction coordinate plots showing apparent activation energies for transitions among 10 bp hairpin conductance states (plots were generated using Table 5 data). The plots compare transitions between IL, UL and LL for 10bp N•N (solid line), 10 bp N•- (dashed line), and 10 bp-•N (dotted line) hairpins. (**A**) 10 bpA•T, 10 bpA•- and 10 bp-•T hairpins; (**B**) 10 bpT•A, 10 bpT•- and 10 bp-•A hairpins; (**C**) 10 bpT•T, 10 bpT•- and 10 bp-•T hairpins.

signatures when captured in the vestibule of the alpha-hemolysin nanopore. Here we refine our model for the general gating mechanism, and further explore possible explanations.

## Depth of pore vestibule probed with angstrom-resolution

We predicted that hairpins ~10 bp or longer would span the pore vestibule, and that detection of differences may be most sensitive to the terminus because of proximity to the strongest part of the potential field. The resistance profile results of 3–12 bp hairpin conductance states suggest that when captured, duplex DNA physically extends from the mouth toward the limiting aperture. The smooth curve fit suggests that the same mechanism accounts for the ionic current blockade caused by all lengths of duplex DNA hairpin molecules. The asymptote at ~10 bp length suggests that this is the length at which the hp stems spans the distance from the vestibule mouth to the limiting aperture. If this is true, then when a 9–10 bp hairpin molecule is captured, the terminal base pair is placed within angstroms of the limiting aperture. Our results showing that DNA hairpins with 9–12 bp stems produce a characteristic four-conductance-state gating pattern when captured in the pore suggests that DNA in this range interacts similarly within the strongest portion of the potential field [i.e. within one radius of the limiting aperture (47)].

Comparison of several alternative models shows that the most likely explanation is the interaction of the terminal bp with residues within the channel vestibule. Three options may explain the gating patterns: (i) the flexibility of the duplex DNA, where DNA molecules with fewer than 9 bp may be too rigid to modulate the ionic current; (ii) extension and retraction along the axis of some or all of the duplex DNA stem or (iii) dynamic interactions between the DNA terminus and protein, each temporary association lasting from one or two to hundreds of milliseconds. The first two models exclude DNA–protein interaction, and this requires that the gating patterns be produced by DNA conformational changes only. This could include DNA stretching induced by the field—the stretching could shift the DNA between B-form and A-form, with A-form allowing more current to flow. This, however, would be expected to produce a two-state blockade. In the second option, the DNA stretching could induce unstacking between base pairs, in which case we would predict multiple blockade states corresponding to each combination of unstacked base pairs. If this were the mechanism, however, we would also anticipate multiple blockade states within events caused by hairpins shorter than 9 bp. With either of these mechanisms, it is difficult to explain how the observed gating occurs only for hairpins 9–12 bp in length, or how the duration of states would be significantly altered by changes to the terminal nucleotides. The results of this study are consistent with the third option, where the conductance states observed with 9 and 10 bp hairpins are due to specific orientation and binding states of the DNA duplex in the pore vestibule, without significantly altering the global structure of the molecule. This model is further supported by the following. Proteins and DNA undergo thermal fluctuations on the same microsecond-to-second time scale we observed for the gating transitions (48,49).

The conformational changes occurring in the DNA and DNA–protein interactions do not have to be large to cause the gating transitions observed. A range of motion occurring within 0.5–1.0 Å is sufficient to have significant affects on the energetics of ion permeation (50). Additionally, the $\Delta G$ values determined are consistent with DNA configurational changes and protein–DNA interactions (51,52).

Our model states that the 3′ and 5′ ends interact with the protein channel with distinct mechanisms, individually and in combination, to produce the three millisecond time scale conductance states of a single 9 bp DNA hairpin molecule blockade. These changes may or may not be sensitive to the calculated bulk free energy of each molecule. We tested this by varying the 3′ and 5′ ends individually as single nucleotide overhangs and together as base pairs to determine the contribution from each and to determine whether the contributions are additive or synergistic in any way. We expected 5′ and 3′ ends to produce a difference even with the same charge or nucleotide because of the different geometrical orientation of each end. We also expected different residues at the same end to have different interactions.

We found that the 3′ and 5′ ends individually produced different changes to the ionic current gating signatures, indicating that a different type of interaction occurs between each end and the protein channel under the potential field. When the individual contributions of the 3′ and 5′ end are compared with the gating signature of the corresponding terminal base pair, the changes are not additive, but appear to be synergistic for at least the lower level. The LL changes correlate directly with the free energy differences among the base paired molecules, but not among the molecules with single nucleotide overhangs. The UL and IL each appear to be dominated by the interaction of 3′ end, even when the base pair is present. The conductance state changes for UL and IL do not directly correlate with the free energy differences among the molecules. There is not a direct relationship between the change in the nucleotide composition and change in gating signal.

## IL, UL and LL

Kinetic analysis of the ionic current gating patterns showed that the dwell time pattern for each DNA hairpin molecule examined was unique and distinguishable from the others. For each conductance state, trends in the affect from altering the terminal position were discernable. We interpret the duration in a conductance state as reflecting the stability of that state (53). Overall, the dwell times for UL, IL and LL for the 10 bp hairpins with Watson–Crick base pairing along the stem were nearly all greater than values obtained for the 9 bpC•G and corresponding overhang hairpins. Among the three conductance states UL, IL and LL, dwell time changes differed in magnitude. LL dwell times changed more than IL or UL, indicating that LL is more sensitive to nucleotide orientation and identity.

For the intermediate level, hydrogen bonding between terminal nucleotides appears to have minimal affect. Although the mismatch TT with reduced H-bonding produced IL with shorter duration than did the terminal base pairs, this may be due to destabilizing affect of T in the 5′ position rather than lack of H-bonding. Future work to test the mismatch C:C could determine whether this effect is

pyrimidine-dependent, or specific to the thymine. We conclude that in addition to the electrostatic interactions that are an important part of IL stability, the ribose sugar and nucleotide also modulate the stability. These results provide experimental evidence that the 3′ end is more available to interact with the pore interior when the hairpin is in the IL-producing conformation.

Our model predicted that UL corresponds to the DNA molecule desorbing from the pore, orienting along the central axis of the channel, and allowing more current to flow. We would expect that increasing the charge at the terminus would favor DNA orientation along the central axis, and thus increase the duration of UL conductance state. Because our model predicted that this state does not depend on interactions between the pore and the DNA, we also would expect that UL duration would be less dependent on base pair identity or orientation. Our results show that the terminal hydrogen-bonded base pair has a much greater affect than phosphate, abasic or nucleotide overhangs, and reveal a slight dependence on the presence of charge and structure in the 3′ position. The presence of the nucleotide base may reduce $\tau_{UL}$ by altering the interaction between the DNA backbone and the ionic current. These results remain consistent with our model of the UL, where the DNA molecule is not directly interacting with the vestibule.

Our model predicted that LL is dependent on base pair identity and orientation, due to interaction of both the 3′ and 5′ ends of the DNA terminus with amino acid residues within the pore vestibule. In our investigation here, we found that the phosphate charge and abasic affected LL durations differently depending on the side on which they were present. The magnitude of duration changes were much greater than those observed for the other conductance states. These results are consistent with our model, where both ends interact with the protein.

The difference in conductance level amplitude between IL and LL may be due the geometry of the DNA molecule. In the 3D structure of an ideal 10–12 bp B-form dsDNA hairpin, the 3′ end has a negative inclination of several degrees from the helix axis (54) (http://www.imb-jena.de/ImgLibDoc/nana/IMAGE_NASP.html). This asymmetric orientation means that an interaction between the limiting aperture and the 5′ end or the 3′ end could causes the molecule to block the flow of ionic current differently. We propose that the IL conductance state results when the 3′ end associates with the limiting aperture, and the 5′ end remains unbound and does not have sufficient length to influence the strong field at the limiting aperture. Alternatively, if the 5′ end binds at or near the limiting aperture, the 3′ end is within angstroms of the limiting aperture, and therefore in the range to interact with amino acid residues. This causes a greater current blockade since both ends influence the current flow which we observe as the LL conductance state.

To summarize the model, the UL results from the DNA hairpin residing unbound in the pore vestibule, the IL conductance state is due to the 3′ end of a duplex interacting with the amino acids at or near the limiting aperture of the protein, while the LL conductance state is a consequence of DNA–protein interactions with both 5′ and 3′ ends.

One explanation for the ion channel sensitivity to nucleotide composition may be the interaction of nucleotide-specific DNA conformational changes with the specific residues at the channel limiting aperture that are responsible for the channel's slight anionic selectivity (55). The pair of two charged residues, E111 and K147, form the highest energetic barrier located in the narrowest part of the channel (36). Site-directed mutagenesis has also demonstrated the role of these residues in ion selectivity (56,57). Because these residues define the limiting aperture, and regulate the anion selectivity, it may be these residues that influence the stability, or durations, of the conductance states caused by DNA hps captured in the pore vestibule.

An additional consideration is the degree to which a captured DNA molecule may organize water molecules in the pore. While water in the unoccupied pore is essentially bulk phase (35,36), captured DNA occupies volume within the vestibule, and alters the charge distribution along the axis of the channel. The organization of water molecules by the spine of the DNA may affect current conductance while the hairpin molecule moves among the proposed configurations in the vestibule. However, for this to be true, the global change in water molecule organization along the DNA molecule would have to also be influenced by the terminus composition, because differences in conductance correspond to local differences at the DNA hp terminus.

It is striking that seemingly minor changes in hairpin association with the pore can produce such significant effects on ionic conductance. In this regard, it is interesting to compare the gating effects demonstrated here with those observed in ligand-gated ion channels of biological membranes, such as the acetylcholine, GABA, NMDA and glycine receptors that mediate synaptic neurotransmission [for references and nucleic acid and protein sequences, see (58)]. For instance, the acetylcholine receptor contains five protein subunits that form a transmembrane pore. When acetylcholine binds to the receptor, the configuration of the transmembrane portion is altered in such a way that the pore opens and allows sodium ions to flow down an electrochemical gradient across the membrane and into the cell.

It is not yet understood how small changes in pore geometry alter the conductance of AChR or other ligand-gated receptors. However, structural information can accelerate the understanding of structural and functional relationships (59). By analogy, we might think of the hemolysin heptamer as a receptor for DNA hairpins. Here, the vestibule is the binding site and the hairpin is the ligand. Because the geometries of the hemolysin pore and hairpin are known at atomic resolution from X-ray diffraction studies, it may be possible to use the hemolysin–hairpin interaction to better understand how subtle changes in molecular architecture of a channel can precisely control ionic current through the pore.

## CONCLUSION

We conclude that the alpha-hemolysin nanopore detection of differences among individual DNA molecules may be more sensitive than other methods to DNA terminus dynamics. This includes nucleotide and base pair conformation and specific components that contribute to individual molecule stability, such as stacking and hydrogen bonding. The nanopore is sensitive to more features than we can currently

explain with simple bulk phase description of the kinetics and thermodynamics. Further analysis of the contributions to stability may be necessary to determine completely the molecular interactions that can explain the blockade gating patterns produced.

Taken together, the conductance states' dwell time responses for DNA hairpins captured in the alpha-hemolysin vestibule show that every single terminal nucleotide overhang influences at least one of the conductance states. The location of the nucleotide, either on the 5′ or 3′ end, governs transitions among conductance states. The dwell time and apparent activation energy results support a model wherein IL is due to the 3′ end of the DNA hairpin interacting with amino acids at or near the limiting aperture, UL is due to an unbound orientation along the central axis of the channel, and LL results from interactions of both the 3′ and 5′ end at or near the limiting aperture. Our proposed explanation for DNA-modulated ionic current in an ion channel detector is intended to provide further context for predicting and interpreting DNA detection using nanopore detectors. Because the alpha-hemolysin ion channel structure is known, and the molecular structure of DNA is well characterized, this system may also prove useful as a model of ligand-gated ion channels.

## ACKNOWLEDGEMENTS

## REFERENCES

1. Wang,L., Hingerty,B.E., Srinivasan,A.R., Olson,W.K. and Broyde,S. (2002) Accurate representation of B-DNA double helical structure with implicit solvent and counterions. *Biophys. J.*, **83**, 382–406.
2. Renisio,J.G., Cosquer,S., Cherrak,I., Antri,S.E., Mauffret,O. and Fermandjian,S. (2005) Pre-organized structure of viral DNA at the binding-processing site of HIV-1 integrase. *Nucleic Acids Res.*, **33**, 1970–1981.
3. Ng,H.-L. and Dickerson,R.E. (2002) Mediation of the A/B-DNA helix transition by G-tracts in the crystal structure of duplex CATGGGCCCATG. *Nucleic Acids Res.*, **30**, 4061–4067.
4. Wu,Z.G., Delaglio,F., Tjandra,N., Zhurkin,V.B. and Bax,A. (2003) Overall structure and sugar dynamics of a DNA dodecamer from homo- and heteronuclear dipolar couplings and P-31 chemical shift anisotropy. *J. Biomol. NMR*, **26**, 297–315.
5. Drew,H.R., Wing,R.M., Takano,T., Broka,C., Tanaka,S., Itakura,K. and Dickerson,R.E. (1981) Structure of a B-DNA dodecamer: conformation and dynamics. *Proc. Natl Acad. Sci. USA*, **78**, 2179–2183.
6. Wartell,R.M. and Benight,A.S. (1985) Thermal denaturation of DNA molecules: a comparison of theory with experiment. *Phys. Rep.*, **126**, 67–107.
7. Vallone,P.M., Paner,T.M., Hilario,J., Lane,M.J., Faldasz,B.D. and Benight,A.S. (1999) Melting studies of short DNA hairpins: influence of loop sequence and adjoining base pair identity on hairpin thermodynamics. *Biopolymers*, **50**, 425–442.
8. Senior,M., Jones,R.A. and Breslauer,K.J. (1988) Influence of dangling thymidine residues on the stability and structure of two DNA duplexes. *Biochemistry*, **27**, 3879–3885.
9. SantaLucia,J., Jr (1998) A unified view of polymer, dumbbell, and oligonucleotide DNA nearest- neighbor thermodynamics. *Proc. Natl Acad. Sci. USA*, **95**, 1460–1465.
10. Bonnet,G., Krichevsky,O. and Libchaber,A. (1998) Kinetics of conformational fluctuations in DNA hairpin-loops. *Proc. Natl Acad. Sci. USA*, **95**, 8602–8606.
11. Elson,E.L., Scheffler,I.E. and Baldwin,R.L. (1970) Helix formation by d(TA) oligomers. 3. Electrostatic effects. *J. Mol. Biol.*, **30**, 17–37.
12. Alberts,B., Bray,D., Lewis,J., Raff,M., Roberts,K. and Watson,J.D. (1994) *Molecular Biology of the Cell*. Garland Publishing, NY.
13. Rief,M., Clausen-Schaumann,H. and Gaub,H.E. (1999) Sequence-dependent mechanics of single DNA molecules. *Nature Struct. Biol.*, **6**, 346–349.
14. Woodside,M.T., Behnke-Parks,W.M., Larizadeh,K., Travers,K., Herschlag,D. and Block,S.M. (2006) Nanomechanical measurements of the sequence-dependent folding landscapes of single nucleic acid hairpins. *Proc. Natl Acad. Sci. USA*, **103**, 6190–6195.
15. Aalberts,D.P., Parman,J.M. and Goddard,N.L. (2003) Single-strand stacking free energy from DNA beacon kinetics. *Biophys. J.*, **84**, 3212–3217.
16. Vercoutere,W., Winters-Hilt,S., Olsen,H., Deamer,D., Haussler,D. and Akeson,M. (2001) Rapid discrimination among individual DNA hairpin molecules at single- nucleotide resolution using an ion channel. *Nat. Biotechnol.*, **19**, 248–252.
17. Vercoutere,W.A., Winters-Hilt,S., DeGuzman,V.S., Deamer,D., Ridino,S.E., Rodgers,J.T., Olsen,H.E., Marziali,A. and Akeson,M. (2003) Discrimination among individual Watson–Crick base pairs at the termini of single DNA hairpin molecules. *Nucleic Acids Res.*, **31**, 1311–1318.
18. Akeson,M., Branton,D., Kasianowicz,J.J., Brandin,E. and Deamer,D.W. (1999) Microsecond time-scale discrimination among polycytidylic acid, polyadenylic acid, and polyuridylic acid as homopolymers or as segments within single RNA molecules. *Biophys. J.*, **77**, 3227–3233.
19. Meller,A., Nivon,L. and Branton,D. (2001) Voltage-driven DNA translocations through a nanopore. *Phys. Rev. Lett.*, **86**, 3435–3439.
20. Li,J.L., Stein,D., Qun,C., Brandin,E., Huang,A., Wang,H., Branton,D. and Golovchenko,J. (2003) Solid state nanopore as a single DNA molecule detector. *Biophys. J.*, **84**, 134A–135A.
21. Deamer,D.W. and Branton,D. (2002) Characterization of nucleic acids by nanopore analysis. *Acc. Chem. Res.*, **35**, 817–825.
22. Aksimentiev,A., Heng,J.B., Timp,G. and Schulten,K. (2004) Microscopic kinetics of DNA translocation through synthetic nanopores. *Biophys. J.*, **87**, 2086–2097.
23. Heng,J.B., Ho,C., Kim,T., Timp,R., Aksimentiev,A., Grinkova,Y.V., Sligar,S., Schulten,K. and Timp,G. (2004) Sizing DNA using a nanometer-diameter pore. *Biophys. J.*, **87**, 2905–2911.
24. Storm,A.J., Storm,C., Chen,J., Zandbergen,H., Joanny,J.-F. and Dekker,C. (2005) Fast DNA translocation through a solid-state nanopore. *Nano Lett.*, **5**, 1193–1197.
25. Kasianowicz,J.J., Brandin,E., Branton,D. and Deamer,D.W. (1996) Characterization of individual polynucleotide molecules using a membrane channel. *Proc. Natl Acad. Sci. USA*, **93**, 13770–13773.
26. Winters-Hilt,S., Vercoutere,W., DeGuzman,V.S., Deamer,D., Akeson,M. and Haussler,D. (2003) Highly accurate classification of Watson–Crick basepairs on termini of single DNA molecules. *Biophys. J.*, **84**, 967–976.
27. Song,L., Hobaugh,M.R., Shustak,C., Cheley,S., Bayley,H. and Gouaux,J.E. (1996) Structure of staphylococcal alpha-hemolysin, a heptameric transmembrane pore [see comments]. *Science*, **274**, 1859–1866.
28. Wang,H., Dunning,J.E., Huang,A.P.-H., Nyamwanda,J.A. and Branton,D. (2004) DNA heterogeneity and phosphorylation unveiled by single-molecule electrophoresis. *Proc. Natl Acad. Sci. USA*, **101**, 13472–13477.
29. Henrickson,S.E., Misakian,M., Robertson,B. and Kasianowicz,J.J. (2000) Driven DNA transport into an asymmetric nanometer-scale pore. *Phys. Rev. Lett.*, **85**, 3057–3060.
30. Howorka,S., Cheley,S. and Bayley,H. (2001) Sequence-specific detection of individual DNA strands using engineered nanopores. *Nat. Biotechnol.*, **19**, 636–639.

31. Sauer-Budge,A.F., Nyamwanda,J.A., Lubensky,D.K. and Branton,D. (2003) Unzipping kinetics of double-stranded DNA in a nanopore. *Phys. Rev. Lett.*, **90**, 238101–238104.

32. Nakane,J.J., Akeson,M. and Marziali,A. (2003) Nanopore sensors for nucleic acid analysis. *J. Phys. Condens. Matter*, **15**, R1365–R1393.

33. Nakane,J., Wiggin,M. and Marziali,A. (2004) A nanosensor for transmembrane capture and identification of single nucleic acid molecules. *Biophys. J.*, **87**, 615–621.

34. Mathe,J., Visram,H., Viasnoff,V., Rabin,Y. and Meller,A. (2004) Nanopore unzipping of individual DNA hairpin molecules. *Biophys. J.*, **87**, 3205–3212.

35. Paula,S., Akeson,M. and Deamer,D. (1999) Water transport by the bacterial channel alpha-hemolysin. *Biochim. Biophys. Acta*, **1418**, 117–126.

36. Noskov,S.Y., Im,W. and Roux,B. (2004) Ion permeation through the alpha-hemolysin channel: theoretical studies based on brownian dynamics and Poisson-Nernst-Plank Electrodiffusion Theory. *Biophys. J.*, **87**, 2299–2309.

37. Lubensky,D.K. and Nelson,D.R. (1999) Driven polymer translocation through a narrow pore. *Biophys. J.*, **77**, 1824–1838.

38. Muthukumar,M. (1999) Polymer translocation through a hole. *J. Chem. Phys.*, **111**, 10371–10374.

39. Muthukumar,M. and Kong,C.Y. (2006) Simulation of polymer translocation through protein channels. *Proc. Natl Acad. Sci. USA*, **103**, 5273–5278.

40. Flomenbom,O. and Klafter,J. (2003) Single-stranded DNA translocation through a nanopore: a master equation approach. *Phys. Rev. E*, **68**, 041910–041917.

41. Kim,S.H., Panwar,A.S., Kumar,S., Ahn,K.H. and Lee,S.J. (2004) Electrophoresis of a bead-rod chain through a narrow slit: a brownian dynamics study. *J. Chem. Phys.*, **121**, 9116–9122.

42. Matysiak,S., Montesi,A., Pasquali,M., Kolomeisky,A.B. and Clementi,C. (2006) Dynamics of polymer translocation through nanopores: theory meets experiment. *Phys. Rev. Lett.*, **96**, 118101–118104.

43. Cocco,S., Monasson,R. and Marko,J.F. (2001) Force and kinetic barriers to unzipping of the DNA double helix. *Proc. Natl Acad. Sci. USA*, **98**, 8608–8613.

44. Senior,M.M., Jones,R.A. and Breslauer,K.J. (1988) Influence of loop residues on the relative stabilities of DNA hairpin structures. *Proc. Natl Acad. Sci. USA*, **85**, 6242–6246.

45. Zuker,M. (2003) Mfold web server for nucleic acid folding and hybridization prediction. *Nucleic Acids Res.*, **31**, 3406–3415.

46. Colquhoun,D. and Sigworth,F.J. (1983) Fitting and Statistical Analysis of Single Channel Records. In Sakmann,B. and Neher,E. (eds), *Single Channel Recording*. Plenum Press, NY, pp. 191–263.

47. Marziali,A. and Akeson,M. (2001) New DNA sequencing methods. *Ann. Rev. Biomed. Eng.*, **3**, 195–223.

48. Karplus,M. and McCammon,J.A. (1981) The internal dynamics of globular proteins. *CRC Crit. Rev. Biochem.*, **9**, 293–349.

49. Karplus,M. and Petsko,G.A. (1990) Molecular dynamics simulations in biology. *Nature*, **347**, 631–639.

50. Allen,T.W., Andersen,O.S. and Roux,B. (2004) On the importance of atomic fluctuations, protein flexibility, and solvent in ion permeation. *J. Gen. Physiol.*, **124**, 679–690.

51. Ansari,A., Kuznetsov,S.V. and Shen,Y.-Q. (2001) Configurational diffusion down a folding tunnel descirbes the dynamics of DNA hairpins. *Proc Natl Acad. Sci. USA*, **98**, 7771–7776.

52. Bockelmann,U., Thomen,P. and Heslot,F. (2004) Dynamics of DNA duplex formation studied by single molecule force measurements. *Biophys. J.*, **87**, 3388–3396.

53. Hille,B. (1992) *Ionic Channels of Excitable Membranes*. Sinauer Associates, Inc., Sunderland, MA.

54. Blackburn,C.M. and Gait,M.J. (1996) *Nucleic acids in chemistry and biology*. Oxford University Press, NY.

55. Menestrina,G. (1986) Ionic channels formed by *Staphylococcus aureus* alpha-toxin: voltage-dependent inhibition by divalent and tri-valent cations. *J. Membr. Biol.*, **90**, 177–190.

56. Gu,L.Q., Cheley,S. and Bayley,H. (2001) Prolonged residence time of a noncovalent molecular adapter, beta-cyclodextrin, within the lumen of mutant alpha-hemolysin pores. *J. Gen. Physiol.*, **118**, 481–493.

57. Gu,L.Q., Dalla Serra,M., Vincent,J.B., Vigh,G., Cheley,S., Braha,O. and Bayley,H. (2001) Reversal of charge selectivity in transmembrane protein pores by using noncovalent molecular adaptors. *Proc. Natl Acad. Sci. USA*, **97**, 3959–3964.

58. Donizelli,M., Djite,M.-A. and Le Novère,N. (2006) LGICdb: a manually curated sequence database after the genomes. *Nucleic Acids Res.*, **34**, D267–D269.

59. Absalom,N.L., Lewis,T.M. and Schofield,P.R. (2004) Mechanisms of channel gating of the ligand-gated ion channel superfamily inferred from protein structure. *J. Exp. Physiol.*, **89**, 145–153.